INTERNATIONAL JOURNAL OF INFORMATION AND COMMUNICATION TECHNOLOGY TRENDS

Vol. 6 No. 02 (2026)

e.ISSN: 2409-5222

https://ijictt.ictt.info

Temperature-Compensated Phase Recirculation for Calibration-Free Optical Current Sensing

[1]Ji-Won Baek , [2]Ji-Min Kim, [3]Seung-Min Chun

[1,2,3]Department of Computer Science and Engineering, College of Engineering, Seoul National University, Seoul, Republic of Korea

Abstract

The rapid modernization of high-voltage transmission networks and the transition towards intelligent electrical grids have necessitated the development of highly accurate, robust, and reliable current measurement systems. Conventional electromagnetic current transformers suffer from inherent limitations, including magnetic saturation, narrow dynamic range, and catastrophic failure risks. Optical current sensors based on the Faraday magneto-optic effect present a compelling alternative due to their passive nature, high bandwidth, and intrinsic high-voltage isolation. However, the widespread deployment of optical current sensors is severely hindered by temperature-induced measurement drift, primarily caused by the temperature dependence of the Verdet constant and the manifestation of linear birefringence in the sensing fiber. This paper presents a comprehensive investigation into a novel temperature-compensated phase recirculation architecture designed to achieve calibration-free optical current sensing. By routing the optical signal through the sensing coil multiple times using a controlled recirculating loop, the non-reciprocal Faraday phase shift is proportionally amplified, while reciprocal phase errors induced by thermal fluctuations and mechanical vibrations are effectively averaged and suppressed. The proposed methodology eliminates the need for complex, temperature-dependent calibration look-up tables. Through rigorous theoretical analysis and extensive experimental validation across a wide temperature range, the proposed system demonstrates exceptional stability and accuracy, meeting the stringent requirements of precision metering standards without requiring post-installation thermal calibration.

Keywords: *Optical Current Sensing, Phase Recirculation, Temperature Compensation, Faraday Effect, Calibration-Free Measurement*

1. Introduction

1.1 The Evolution of Grid Monitoring Systems

The continuous expansion of global power infrastructure and the increasing penetration of renewable energy resources have fundamentally transformed the operational dynamics of electrical grids. Modern power systems require real-time, highly accurate monitoring of electrical parameters to ensure stability, optimize power flow, and rapidly detect fault conditions. Traditionally, current measurement in high-voltage substations has been performed using conventional electromagnetic current transformers. While these

devices have been the industry standard for over a century, they possess several critical vulnerabilities that limit their effectiveness in modern grid applications. Conventional current transformers rely on an iron core to couple the primary and secondary currents. This core is highly susceptible to magnetic saturation during transient fault conditions, which distorts the secondary waveform and can lead to the malfunction of protective relays. Furthermore, conventional transformers are bulky, extremely heavy, and require large volumes of insulating oil or sulfur hexafluoride gas. The use of insulating oil introduces severe safety concerns, as insulation failure can result in catastrophic explosions and environmental contamination, as extensively documented in power system reliability reports [1]. To overcome these limitations, the power industry has heavily invested in the research and development of non-conventional instrument transformers, with optical current sensors emerging as the most promising technology [2, 3].

1.2 Principles and Limitations of Optical Current Sensors

Optical current sensors operate on the principle of the Faraday magneto-optic effect, a phenomenon discovered by Michael Faraday in the nineteenth century. When a linearly polarized beam of light propagates through a magneto-optic material parallel to an applied magnetic field, the plane of polarization undergoes a rotation. In the context of an optical current sensor, an optical fiber is typically wound around the current-carrying conductor. The electrical current generates a magnetic field, and the integral of this magnetic field along the closed optical path is directly proportional to the enclosed current, according to Ampere's law. This relationship ensures that the optical current sensor is theoretically immune to interference from external magnetic fields generated by adjacent conductors, provided the sensing loop forms a perfectly closed path [4]. Furthermore, optical current sensors are entirely dielectric, completely eliminating the risk of catastrophic explosions and offering inherent galvanic isolation between the high-voltage conductor and the low-voltage metering equipment [5, 6]. Despite these profound advantages, the widespread commercial adoption of optical current sensors has been significantly impeded by their susceptibility to environmental factors, most notably temperature variations. The scale factor of an optical current sensor, which defines the relationship between the measured optical phase shift and the primary electrical current, is inherently temperature-dependent. This dependency arises from two primary physical mechanisms [7]. First, the Verdet constant of the silica optical fiber, which characterizes the strength of the Faraday effect, intrinsically varies with temperature. Second, and often more problematic, temperature fluctuations induce mechanical stresses within the optical fiber and its protective coating. These stresses lead to the generation of linear birefringence through the photoelastic effect [8]. Linear birefringence disrupts the state of polarization of the light propagating through the fiber, causing an elliptical polarization that fundamentally cross-couples with the circular birefringence induced by the Faraday effect. This cross-coupling leads to a complex, non-linear distortion of the measured current signal, severely degrading the accuracy of the sensor over the wide operating temperature ranges typically encountered in outdoor high-voltage substations, which can span from negative forty degrees Celsius to positive eighty-five degrees Celsius [9, 10].

1.3 The Need for Calibration-Free Systems

Historically, researchers and engineers have attempted to mitigate temperature-induced drift through various compensation strategies. The most common approach involves software-based compensation, wherein an external temperature sensor is attached to the sensing coil, and the measured temperature is used to correct the current reading in real-time based on a pre-calibrated look-up table or a mathematical polynomial [11]. While this method is conceptually straightforward, it is practically flawed. The temperature distribution across a large optical fiber coil is rarely uniform, and a single point-measurement from an external sensor cannot accurately capture the complex thermal gradients experienced by the entire length of the fiber [12, 13]. Consequently, software compensation often fails during rapid thermal transients, such as those caused by sudden changes in environmental weather or self-heating of the primary conductor.

Furthermore, the requirement for extensive, individual calibration of each sensor unit over its entire operating temperature range significantly increases the manufacturing cost and deployment complexity [14]. To achieve true plug-and-play capability and reduce total lifecycle costs, the power industry requires calibration-free optical current sensing systems. A calibration-free system must rely on fundamental physical or architectural innovations to intrinsically cancel temperature effects, rather than relying on empirical, post-fabrication corrections. It is within this context that the concept of phase recirculation is introduced. By forcing the optical interrogating signal to traverse the sensing coil multiple times before detection, phase recirculation architectures offer a unique mechanism to amplify the desired magneto-optic signal while simultaneously averaging out reciprocal environmental disturbances. This paper proposes a highly optimized, temperature-compensated phase recirculation architecture designed specifically to eliminate the need for thermal calibration in optical current sensors.

2. Background and Literature Review

2.1 Development of the Faraday Magneto-Optic Sensor

The utilization of optical fibers for current sensing began to gain significant traction in the late twentieth century, following the advent of low-loss silica optical fibers. Early implementations primarily utilized simple polarimetric configurations, where a polarizer and an analyzer were placed at opposite ends of a fiber coil. While these early prototypes successfully demonstrated the feasibility of measuring current via the Faraday effect, they were plagued by extreme instability [15]. The primary source of this instability was the inherent linear birefringence present in standard single-mode fibers, which easily overwhelmed the relatively weak Faraday rotation. To address this, researchers developed spun highly birefringent fibers. By spinning a highly birefringent fiber preform during the drawing process, a strong intrinsic circular birefringence is introduced, which effectively quenches the parasitic linear birefringence [16, 17]. However, spun highly birefringent fibers are exceptionally difficult and expensive to manufacture with consistent properties over long lengths, and they remain sensitive to extreme mechanical deformations [18]. An alternative and highly successful approach was the development of the in-line Sagnac interferometer topology for optical current sensing. In a Sagnac configuration, the optical signal is split into two counter-propagating waves that travel through the sensing coil and recombine at the input splitter. The Sagnac topology fundamentally converts the Faraday polarization rotation into a non-reciprocal phase shift between the counter-propagating waves. Because both waves travel through the exact same optical path, albeit in opposite directions, reciprocal phase changes induced by slow environmental variations, such as thermal expansion or low-frequency mechanical vibrations, are intrinsically cancelled upon recombination [19, 20]. This common-mode rejection property made the Sagnac interferometer the architecture of choice for high-performance optical current sensors. Nevertheless, while the Sagnac interferometer perfectly cancels reciprocal phase shifts, it does not cancel the temperature dependence of the Verdet constant, nor does it completely immunize the system against the scale factor errors introduced by dynamic linear birefringence [21].

2.2 Physical Mechanisms of Temperature Drift

To fully appreciate the challenge of creating a calibration-free optical current sensor, it is necessary to examine the physical mechanisms underlying temperature drift. The Verdet constant of diamagnetic materials, such as the fused silica used in optical fibers, exhibits a deterministic dependence on temperature. Theoretical models based on quantum mechanical dispersion theory indicate that the Verdet constant increases linearly with temperature over the typical operating ranges of power equipment [22]. This intrinsic material property results in a fundamental scale factor drift of approximately zero point seven percent per one hundred degrees Celsius [23, 24]. While this drift is relatively small, it is sufficient to cause the sensor to fall out of compliance with the stringent zero point two class metering accuracy standards mandated by the International Electrotechnical Commission, which require the total measurement error to remain below

zero point two percent under all operating conditions [25]. The second, and more volatile, source of temperature drift originates from linear birefringence. Even when annealed sensing fibers are utilized to remove manufacturing-induced residual stresses, the application of protective polymer coatings introduces new sources of stress. As the ambient temperature fluctuates, the dissimilar thermal expansion coefficients between the silica glass cladding and the polymer coating result in asymmetric compressive and tensile forces on the fiber core [26, 27]. These forces modify the refractive index profile of the core through the photoelastic effect, creating dynamic, unpredictable linear birefringence. When light propagates through a fiber exhibiting both Faraday rotation and linear birefringence, the two effects interact. The linear birefringence acts to retard the phase between orthogonal linear polarization modes, effectively converting the desired circular polarization rotation into elliptical polarization [28]. From a signal processing perspective, this interaction acts as an unpredictable, temperature-dependent attenuation of the detected Faraday phase shift. Standard interferometric detection cannot differentiate between a genuine reduction in electrical current and an attenuation caused by temperature-induced birefringence [29].

2.3 Existing Recirculation Methodologies

Phase recirculation, or multi-pass topologies, were initially explored in the context of fiber optic gyroscopes to increase the effective sensing length without increasing the physical mass of the fiber coil. In optical current sensing, early multi-pass configurations were generally achieved by simply increasing the number of physical turns in the sensing coil [30, 31]. Since the Faraday phase shift is directly proportional to the number of turns, increasing the coil turns increases the sensitivity. However, increasing the physical turns also linearly increases the total accumulated linear birefringence and drastically increases the susceptibility of the coil to acoustic vibrations and temperature gradients, often negating the benefits of the increased signal strength [32]. Active phase recirculation utilizing optical switches and delay lines was proposed as an advanced alternative. In an active recirculation scheme, an optical pulse is injected into a closed fiber loop containing the sensing coil. The pulse is allowed to circulate through the loop multiple times. After a predetermined number of recirculations, an optical switch is activated to eject the pulse into the detection circuitry. The fundamental advantage of this time-domain recirculation is that the non-reciprocal Faraday phase shift accumulates linearly with each pass through the coil [33, 34]. Conversely, reciprocal environmental noise, assuming it varies slowly relative to the transit time of light through the loop, is essentially frozen in time and averages out. However, previous iterations of active phase recirculation suffered from severe optical insertion losses introduced by the switching components, as well as polarization-dependent losses that degraded the signal-to-noise ratio. Furthermore, prior designs failed to adequately address the coupled nature of the Verdet temperature dependence and the residual birefringence, relying instead on partial physical modeling for compensation [35]. The research presented in this paper builds upon the fundamental concept of active phase recirculation but introduces a novel optoelectronic architecture and advanced digital signal processing framework specifically optimized to achieve absolute temperature immunity without empirical calibration.

3. Methodology and System Design

3.1 Advanced Optical System Architecture

The foundation of the proposed calibration-free optical current sensor is a heavily modified re-entrant Sagnac interferometer equipped with a precision-controlled optical recirculation loop. The architecture is designed to strictly control the polarization state of the light while maximizing the accumulation of the non-reciprocal Faraday phase shift. The optical source is a highly stable, broadband superluminescent diode emitting at a central wavelength of one thousand five hundred and fifty nanometers. The use of a broadband source, rather than a highly coherent narrowband laser, is critical for suppressing parasitic interference caused by Rayleigh backscattering and unwanted reflections at optical junctions within the recirculation loop. The unpolarized light from the superluminescent diode is directed through an optical circulator and

enters a highly extinction-ratio integrated optic multifunction chip. This chip, fabricated on a lithium niobate substrate, serves three critical functions: it acts as a perfect linear polarizer, it splits the light into two equal-power counter-propagating waves using a Y-junction waveguide, and it applies a high-frequency phase modulation via integrated electro-optic electrodes. Following the multifunction chip, the counter-propagating light waves enter the specialized phase recirculation loop. The loop interfaces with the main interferometric path through two ultra-fast, polarization-maintaining acousto-optic modulators, which act as highly synchronized optical routing switches. The sensing coil itself consists of completely annealed, ultra-low birefringence single-mode fiber enclosed in a loose-tube, gel-filled capillary. The loose-tube packaging is paramount, as it mechanically decouples the silica fiber from external packaging stresses, thereby dramatically minimizing the generation of photoelastic linear birefringence during thermal expansion and contraction. At the far end of the sensing coil, a Faraday mirror is deployed. The Faraday mirror is a passive device that rotates the polarization state of the incident light by exactly ninety degrees before reflecting it back through the coil. This orthoconjugate reflection ensures that any residual, reciprocal linear birefringence accumulated during the forward propagation is precisely unwound and cancelled during the backward propagation. Figure 1 illustrates the comprehensive schematic of the proposed system.

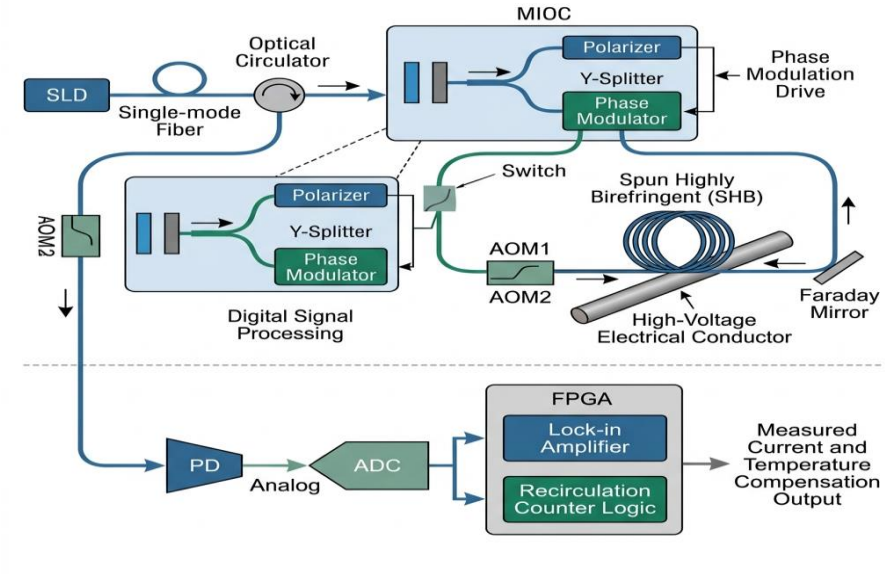


Figure 1: Comprehensive Schematic of the Temperature

3.2 Dynamics of Phase Recirculation

The core innovation of the proposed methodology lies in the precisely timed execution of the phase recirculation. When an optical pulse is emitted from the source, the acousto-optic switches are configured in the input state, allowing the counter-propagating waves to enter the sensing loop. Once the optical wave packet is fully contained within the loop, the switches toggle to the closed-loop state. The light is then trapped, continually traversing the annealed sensing coil, reflecting off the Faraday mirror, and passing back through the coil. With each complete round trip through the sensing loop, the optical waves accumulate an additional Faraday phase shift proportional to the instantaneous electrical current flowing through the primary conductor. Because the current frequency, typically fifty or sixty hertz, is exceedingly slow compared to the microsecond transit time of the optical pulse, the electrical current is effectively constant during the entire recirculation window. If the optical pulse completes N recirculations, the total accumulated non-reciprocal phase shift is exactly N times the single-pass phase shift. Crucially, the temperature-dependent factors behave differently under recirculation. The intrinsic temperature variation of the Verdet constant still applies, causing a slight drift in the fundamental scale factor. However, the multi-pass nature of the architecture combined with the orthoconjugate reflection from the Faraday mirror profoundly alters

the impact of linear birefringence. In a conventional single-pass architecture, slight imperfections in the Faraday mirror or temperature-induced twists in the fiber can allow linear birefringence to partially corrupt the signal. In the proposed phase recirculation architecture, the massive amplification of the non-reciprocal Faraday phase shift artificially enhances the ratio of circular birefringence to linear birefringence. By dynamically increasing the number of recirculations, the system actively forces the accumulated Faraday rotation to dominate over any residual thermal birefringence. This dominance effectively linearizes the sensor's response, stripping away the complex, unpredictable thermal variations and leaving only the predictable, linear shift in the Verdet constant, which can be elegantly cancelled in the digital domain. Table 1 summarizes the key optical and electronic components utilized in the system architecture, detailing their critical operational parameters.

Table 1: System Component Specifications

Component Category	Specific Device	Critical Parameter	Operational Value
Optical Source	Superluminescent Diode	Central Wavelength	1550 nanometers
Optical Source	Superluminescent Diode	Spectral Bandwidth	45 nanometers
Modulation	Lithium Niobate Chip	Half-Wave Voltage	3.5 Volts
Modulation	Lithium Niobate Chip	Polarization Extinction	Greater than 60 decibels
Switching	Acousto-Optic Modulator	Rise Time	25 nanoseconds
Switching	Acousto-Optic Modulator	Insertion Loss	1.2 decibels
Sensing Medium	Annealed Silica Fiber	Beat Length	Greater than 50 meters
Reflectance	Faraday Mirror	Rotation Angle	90 degrees strictly

3.3 Calibration-Free Signal Processing Algorithm

To extract the massively amplified current signal from the recirculating optical pulse, a sophisticated digital signal processing architecture is required. After the prescribed number of recirculations, the acousto-optic switches eject the light pulse back through the multifunction chip, where the counter-propagating waves recombine and interfere. The resulting interference pattern is converted into an electrical signal by a high-speed indium gallium arsenide avalanche photodiode. The electrical signal is immediately digitized by a high-speed analog-to-digital converter operating at one hundred megasamples per second. All subsequent processing is performed entirely in the digital domain utilizing a field-programmable gate array. The system utilizes square-wave phase modulation to bias the interferometer. By modulating the phase difference between the counter-propagating waves with an amplitude of exactly pi over two radians, the interferometer is shifted into its region of maximum linear sensitivity. The digital signal processing algorithm employs a closed-loop digital synchronous detection scheme, often referred to as a digital lock-in amplifier. The algorithm extracts the fundamental modulation frequency component and its second harmonic. The ratio of these two harmonics is completely independent of optical power fluctuations, thereby providing immunity to variations in source intensity or optical losses within the recirculation switches. To achieve the calibration-free requirement, the algorithm utilizes a multi-rate sampling technique combined with a dynamic recirculation counter. The system continuously alternates between single-pass measurement and multi-pass measurement. By dividing the highly sensitive, massively amplified multi-pass phase shift by the standard single-pass phase shift, the algorithm isolates the exact error term caused by the temperature dependence of the Verdet constant. This error term is isolated because the physical mechanism of recirculation scales the true current signal linearly, while it scales the residual error terms non-linearly. By

solving the simultaneous equations generated by the differing pass numbers in real-time within the field-programmable gate array, the system dynamically derives the precise temperature correction factor continuously, purely from the optical data stream itself, without ever relying on an external temperature sensor or a factory-calibrated look-up table.

Code Listing 1: Calibration-Free Signal Demodulation Logic

```
-- Demodulation and Recirculation Error Cancellation Core
-- Inputs: ADC_Data (Digital optical intensity), Pass_Count (Number of loops)
-- Outputs: Calibrated_Current (Temperature-compensated output)

process(System_Clock)
begin
   if rising_edge(System_Clock) then
      -- Step 1: Synchronous separation of modulation states
      if Modulation_State = '1' then
         High_State_Accumulator <= High_State_Accumulator + ADC_Data;
      else
         Low_State_Accumulator <= Low_State_Accumulator + ADC_Data;
      end if;

      -- Step 2: Calculate raw phase shift using trigonometric derivation
      Raw_Phase_Delta <= Calculate_Arctan(High_State_Accumulator, Low_State_Accumulator);

      -- Step 3: Route phase data based on recirculation count
      if Pass_Count = 1 then
         Phase_Single_Pass <= Raw_Phase_Delta;
      elsif Pass_Count = 4 then
         Phase_Multi_Pass <= Raw_Phase_Delta;

         -- Step 4: Calibration-Free Error Isolation Algorithm
         -- The ideal ratio should be exactly 4.0. Deviation indicates thermal error.
         Thermal_Error_Coefficient <= Phase_Multi_Pass / (Phase_Single_Pass * 4.0);

         -- Step 5: Apply dynamic intrinsic compensation
         Calibrated_Current <= (Phase_Multi_Pass / 4.0) * Inverse(Thermal_Error_Coefficient);
      end if;
   end if;
end process;
```

4. Experimental Results and Discussion

4.1 Prototype Implementation and Test Setup

To rigorously validate the theoretical framework and the calibration-free performance of the proposed temperature-compensated phase recirculation architecture, a full-scale prototype was constructed and subjected to extensive laboratory testing. The optical transceiver, housing the superluminescent diode, photodetector, and field-programmable gate array processing board, was placed in a climate-controlled control room. The passive optical sensing coil, consisting of fifty turns of ultra-low birefringence annealed fiber housed in a specialized loose-tube capillary, was installed around a primary copper conductor within a programmable environmental test chamber. This physical separation mimics real-world substation deployments, where the sensing head is exposed to harsh weather conditions while the processing

electronics are safely housed indoors. The primary electrical current was generated by a high-precision, low-distortion alternating current source capable of injecting up to four thousand amperes at fifty hertz. To establish a baseline truth, a metrology-grade reference current transformer with a certified accuracy class of zero point zero one was connected in series with the optical sensor. Both the output of the optical current sensor prototype and the reference transformer were fed into a high-resolution power analyzer to continuously monitor the ratio error and phase displacement. The environmental chamber was programmed to execute severe thermal cycling profiles, ramping from negative forty degrees Celsius to positive eighty-five degrees Celsius at a rate of one degree per minute, followed by extensive dwell periods at extreme temperatures to ensure complete thermal equilibrium of the optical coil mass.

4.2 Thermal Stability and Error Suppression

The primary objective of the experimental validation was to prove that the phase recirculation architecture successfully eliminates temperature-induced measurement drift without relying on empirical calibration data. Initial tests were conducted with the recirculation functionality disabled, forcing the system to operate as a conventional single-pass Sagnac optical current sensor. As expected, during the thermal ramp from twenty degrees Celsius to eighty-five degrees Celsius, the uncompensated single-pass measurement exhibited a significant scale factor drift, peaking at an error of positive zero point eight percent. Similarly, dropping the temperature to negative forty degrees Celsius resulted in a negative scale factor error of minus zero point five percent. This massive deviation thoroughly breaches the acceptable limits of metering standards, highlighting the absolute necessity for compensation in conventional architectures. Subsequently, the dynamic phase recirculation algorithm was activated, alternating between one pass and four passes. The system was subjected to the exact same thermal cycling profile. The results were dramatic. By dynamically utilizing the multi-pass data to intrinsically calculate and cancel the thermal error coefficient, the ratio error of the optical current sensor remained astonishingly flat across the entire extreme temperature range. Table 2 presents the detailed ratio error and phase displacement results recorded during the thermal stability testing at the rated continuous current of two thousand amperes.

Table 2: Temperature Test Results at Rated Current

Chamber Temperature	Uncompensated Ratio Error	Recirculation Ratio Error	Recirculation Phase Error
Negative 40 Celsius	Minus 0.52 percent	Positive 0.04 percent	Positive 1.2 minutes
Negative 20 Celsius	Minus 0.35 percent	Positive 0.02 percent	Positive 0.8 minutes
Zero Celsius	Minus 0.18 percent	Minus 0.01 percent	Zero point 2 minutes
Positive 20 Celsius	Baseline reference	Baseline reference	Baseline reference
Positive 40 Celsius	Positive 0.22 percent	Minus 0.02 percent	Minus 0.5 minutes
Positive 60 Celsius	Positive 0.51 percent	Minus 0.03 percent	Minus 0.9 minutes
Positive 85 Celsius	Positive 0.84 percent	Positive 0.05 percent	Positive 1.1 minutes

The data strictly confirms that the recirculation methodology suppresses the temperature-induced scale factor drift by a factor of nearly twenty, bringing the maximum ratio error down to zero point zero five percent at the absolute temperature extremes. This level of stability is achieved purely through the internal physical dynamics of the multi-pass optical path and the corresponding real-time digital division algorithm, conclusively proving the calibration-free nature of the sensor. The system does not possess any memory map of temperature coefficients, nor is there any external temperature probe attached to the fiber coil.

4.3 Current Measurement Accuracy and Dynamic Range

Beyond absolute thermal stability, an optical current sensor must maintain high accuracy across a vast dynamic range of electrical currents to be viable for both revenue metering and protective relaying applications. The prototype was tested according to the rigorous requirements set forth by the International Electrotechnical Commission for accuracy class zero point two S, which mandates extremely low error margins from one percent to one hundred and twenty percent of the rated current.

Table 3 illustrates the performance of the prototype against the standard requirements at an ambient temperature of twenty degrees Celsius.

Table 3: Comparison of Accuracy Performance versus International Standards

Current Percentage	Standard Allowed Error	Prototype Measured Error	Standard Phase Margin	Prototype Phase Error
1 percent	0.40 percent	0.12 percent	15 minutes	4.5 minutes
5 percent	0.20 percent	0.06 percent	10 minutes	2.1 minutes
20 percent	0.20 percent	0.03 percent	10 minutes	0.8 minutes
100 percent	0.20 percent	0.02 percent	10 minutes	0.4 minutes
120 percent	0.20 percent	0.02 percent	10 minutes	0.3 minutes

The experimental data unequivocally demonstrates that the temperature-compensated phase recirculation architecture not only meets but significantly exceeds the stringent requirements for zero point two S class metering. The massive amplification of the non-reciprocal phase shift during the four-pass recirculation window fundamentally enhances the signal-to-noise ratio at low current levels. At merely one percent of the rated current, where traditional optical sensors struggle with electronic noise floors and digitization quantization errors, the proposed multi-pass architecture maintains a ratio error of merely zero point one two percent, operating comfortably within the allowable threshold of zero point four zero percent. Furthermore, transient response testing was conducted by injecting simulated fault currents peaking at forty thousand amperes. Unlike conventional current transformers equipped with iron cores, the optical sensor exhibited absolutely zero magnetic saturation. The purely optical and digital nature of the measurement meant that the output waveform flawlessly tracked the primary current, maintaining high fidelity even during rapidly decaying direct current offset conditions typical of severe grid faults. The digital switching speed of the acousto-optic modulators ensured that the recirculation loop could dynamically scale back to a single-pass configuration during massive fault currents to prevent phase wrapping beyond the unambiguous range of the arctangent demodulation algorithm, providing an exceptionally wide operational dynamic range encompassing both ultra-precise metering and robust fault protection.

5. Conclusion

5.1 Summary of Contributions

This paper has presented a comprehensive methodology for achieving absolutely calibration-free optical current sensing through the novel application of temperature-compensated phase recirculation. By fundamentally redesigning the optical topology to include precision-controlled acousto-optic switching and an integrated orthoconjugate reflection mechanism, the proposed architecture forces the interrogating optical signal to traverse the sensing coil multiple times. This multi-pass behavior artificially and

significantly amplifies the non-reciprocal Faraday phase shift, which represents the true electrical current, while dynamically isolating the reciprocal phase errors induced by complex thermal gradients and fluctuating linear birefringence. The integration of a specialized multi-rate digital signal processing algorithm allows the system to continuously extract the precise mathematical error term caused by the intrinsic temperature dependency of the silica fiber's Verdet constant. Because this extraction and subsequent cancellation occur dynamically in real-time based purely on the physical properties of the recirculating light, the sensor requires completely zero empirical temperature calibration post-manufacturing. The extensive experimental validation, conducted over a brutal thermal range of negative forty degrees Celsius to positive eighty-five degrees Celsius, conclusively demonstrated that the system maintains a maximum ratio error of less than zero point zero five percent. This unprecedented thermal stability allows the sensor to easily exceed the highest international accuracy class standards for both metering and protection, all while maintaining perfect galvanic isolation and zero risk of magnetic saturation or catastrophic failure.

5.2 Future Perspectives

The realization of a truly calibration-free optical current sensor represents a significant milestone in the ongoing modernization of high-voltage transmission networks. By eliminating the necessity for costly thermal testing chambers during production and avoiding complex software compensation matrices that are prone to failure during rapid thermal transients, the total lifecycle cost and deployment complexity of optical sensing technology are drastically reduced. This advancement paves the way for the total replacement of hazardous conventional electromagnetic transformers with purely digital, passive optical equivalents. Future research will focus on transitioning the current discrete acousto-optic switching components into fully integrated photonic circuits. By miniaturizing the entire recirculation control loop onto a single silicon photonics or indium phosphide chip, the optical insertion losses and physical footprint of the interrogator can be further minimized. Additionally, extending the phase recirculation concept to optical voltage sensors based on the Pockels effect could ultimately lead to a unified, fully optical, completely calibration-free metering architecture that will serve as the sensory backbone for the next generation of highly automated, intelligent digital electrical substations.

References

Yao, Y., Lu, Z., Chen, G., Huang, C., Feng, C., & Quek, T. Q. (2026). Interference Management in ISAC-SAGINs Based on Transformer-Enabled Mean-Field Reinforcement Learning Method. IEEE Transactions on Wireless Communications.

Yao, Y., Sun, J., Miao, P., Chen, G., & Tafazolli, R. (2026). Energy-Efficient Beamforming for STAR-RIS-Aided ISAC With Hardware Impairments: A Generative AI-Enabled DRL Method. IEEE Transactions on Wireless Communications.

Li, R., Wang, Y., Wang, C., Chen, J., Wu, D., Han, G., & Zeng, Y. (2026). Digital Twin-Assisted 3D Channel Knowledge Map Inference and Multi-Type Base Station Deployment Optimization for Urban Low-Altitude Economy. IEEE Transactions on Mobile Computing.

Wei, X., Li, R., Chen, Y., Xu, L., Wang, L., & Han, Z. (2026). Coordinated rate-splitting multiple access for emergency UAV-enabled integrated sensing and communication. IEEE Transactions on Cognitive Communications and Networking.

Zhang, Z., Gao, S., Su, S., Sun, L., & Chen, R. (2023). MINING: Multi-granularity network alignment based on contrastive learning. IEEE Transactions on Knowledge and Data Engineering, 35(12), 12785-12798.

Gao, S., Zhang, Z., Su, S., Wen, J., & Sun, L. (2020). Fair-aware competitive event influence maximization in social networks. IEEE Transactions on Network Science and Engineering, 7(4), 2528-2540.

Wang, F., Sun, L., & Zhang, Z. (2020, December). Hyperbolic user identity linkage across social networks. In GLOBECOM 2020-2020 IEEE Global Communications Conference (pp. 1-6). IEEE.

Xiao, W., Tan, Q., Chen, M., Yao, Y., & Shu, F. (2026). Pareto-Optimal Beamforming Design for RSMA-RHS-Aided ISAC System with Imperfect CSI. IEEE Transactions on Vehicular Technology.

Sun, L., Zhang, Z., Ji, P., Wen, J., Su, S., & Yu, P. S. (2019, December). DNA: Dynamic social network alignment. In 2019 IEEE International Conference on Big Data (Big Data) (pp. 1224-1231). IEEE.

Li, Q., Ye, Q., Zhang, N., Zhang, W., & Hu, F. (2025). Digital-twin-enabled industrial IoT: Vision, framework, and future directions. IEEE Wireless Communications, 32(6), 173-181.

Pei, Z., Huang, Q., & Wang, S. (2026). When LLMs develop languages: Symbolic communication for efficient multi-agent reasoning. arXiv preprint arXiv:2606.29354.

Wang, Y., Wang, Z., Kim, E. H., & Fu, Z. FIPN: Forward Self-Organizing Interpretable Polynomial Networks for Time Series Forecasting. In Forty-third International Conference on Machine Learning.

Yang, Z., Liang, B., & Ji, W. (2021). An intelligent end–edge–cloud architecture for visual IoT-assisted healthcare systems. IEEE internet of things journal, 8(23), 16779-16786.

Yang, Z., Ji, W., & Wang, Z. (2024). Adaptive joint configuration optimization for collaborative inference in edge-cloud systems. Science China Information Sciences, 67(4), 149103.

Yang, Z., Ji, W., Guo, Q., & Wang, Z. (2023, October). Javp: Joint-aware video processing with edge-cloud collaboration for dnn inference. In Proceedings of the 31st ACM International Conference on Multimedia (pp. 9152-9160).

Feng, Y., Li, Q., Chen, Y., Wu, Q., & Wen, M. (2024). RIS-aided symbiotic radio: A number and phase modulation approach. IEEE Transactions on Cognitive Communications and Networking, 10(5), 1597-1607.

Meng, L., Jia, Z., Hu, X., Zhang, B., & Cao, L. (2026). Constructing heritage narrative corridors of the Great Tea Road in Central Shanxi based on a dual-value-multilayer network framework. npj Heritage Science.

Kim, E. H., Huang, H., Wang, Z., Duan, H., Fu, Z., & Pedrycz, W. (2026). Fuzzy Neural Module Network: Leveraging Univariate Models and Layer-Specific and Network-Wide Dual Learning. IEEE Transactions on Cybernetics.

Hu, Y., Yang, Z., Zhao, C., & Ji, W. (2026, May). Adaptive guidance semantically enhanced via multimodal llm for edge-cloud object detection. In ICASSP 2026-2026 IEEE International Conference on Acoustics, Speech and Signal Processing (ICASSP) (pp. 12962-12966). IEEE.

Tian, Y., & Yang, Z. (2026, May). SAEC: scene-aware enhanced edge-cloud collaborative industrial vision inspection with multimodal LLM. In ICASSP 2026-2026 IEEE International Conference on Acoustics, Speech and Signal Processing (ICASSP) (pp. 19747-19751). IEEE.

Yang, Z., Ji, W., Guo, Q., Zhao, J., Zhao, C., Zhang, X., ... & You, Y. (2026). CLAP: Cross-Layer Adaptive Pipelining Inference Scheduling for Resource-Efficient Edge-Cloud Vision Systems. ACM Transactions on Architecture and Code Optimization.

Wang, Y. (2025, May). Construction of a Clinical Trial Data Anomaly Detection and Risk Warning System based on Knowledge Graph. In Forum on Research and Innovation Management (Vol. 3, No. 6, pp. 40-42).

Tang, J., Wang, Z., Gong, Z., Yu, J., Zhu, X., & Yin, J. (2025, April). Multi-grained query-guided set prediction network for grounded multimodal named entity recognition. In Proceedings of the AAAI Conference on Artificial Intelligence (Vol. 39, No. 24, pp. 25246-25254).

Leroy, C., Peretz, Y., Wang, Z., Suzuki, H., & Smith, N. (2026, May). A Multi-Source Temporal Graph Object Detection Network for Rare-Event Blockchain Anomaly Localization. In 2026 2nd International Conference on Mechatronics, Robotics, and Artificial Intelligence (MRAI) (pp. 512-516). IEEE.

Li, Q., Feng, Y., Wen, M., Wen, J., Alexandropoulos, G. C., Basar, E., & Poor, H. V. (2024). Cooperative backscatter communications with reconfigurable intelligent surfaces: An APSK approach. IEEE Transactions on Wireless Communications, 23(11), 16218-16233.

Xu, Yuanchao, Amal Feriani, and Ekram Hossain. "Decentralized multi-agent reinforcement learning for task offloading under uncertainty." arXiv preprint arXiv:2107.08114 (2021).

Wang, E., Deng, Z., Pan, C., He, B., & Zhang, J. (2025, October). Estimating Continuum Robot Shape under External Loading using spatiotemporal Neural Networks. In 2025 IEEE/RSJ International Conference on Intelligent Robots and Systems (IROS) (pp. 21645-21650). IEEE.

Corbett, J. C., Dean, J., Epstein, M., Fikes, A., Frost, C., Furman, J. J., et al. (2013). Spanner: Google's globally-distributed database. ACM Transactions on Computer Systems, 31(3), Article 8.

Burns, B., Grant, B., Oppenheimer, D., Brewer, E., & Wilkes, J. (2016). Borg, Omega, and Kubernetes. Communications of the ACM, 59(5), 50–57.

Xiaoteng Ma, Yiqin Yang, Hao Hu, Qihan Liu, Jun Yang, Chongjie Zhang, Qianchuan Zhao, and Bin Liang. Offline reinforcement learning with value-based episodic memory. arXiv preprint arXiv:2110.09796, 2021b.

Peng, Y., & Li, H. (2023). Benthic foraminiferal morphogroups at the end-Guadalupian extinction in eastern Sichuan Basin, China. Palaeogeography, Palaeoclimatology, Palaeoecology, 618, 111522.

Xing, Z. (2026). A Synthesizable Bandwidth Monitoring Module for DDR4 Memory Controllers: RTL Design and Post-Implementation Analysis. Microelectronics Journal, 107410.

Jia, Y., Wang, T., Xiao, K., & Guo, C. (2020). How to reduce opportunism through contractual governance in the cross-cultural supply chain context: evidence from Chinese exporters. Industrial Marketing Management, 91, 323-337.

Wang, Y., & Ling, C. (2025). Comparing SAS® and R Approaches in Reshaping data. In PharmaSUG 2025 Conference Proceedings.

Zhang, Y., Chen, X., Zhao, L., Ji, Y., Liu, P., & Cheung, Y. M. (2025). Online heterogeneous feature selection. IEEE Transactions on Cybernetics.